# Partially Prism-Gridded FDTD Analysis for Layered Structures of Transversely Curved Boundary

Chieh-Tsao Hwang, Shau-Gang Mao, *Member, IEEE*, Ruey-Beei Wu, *Senior Member, IEEE*, and Chun-Hsiung Chen, *Fellow, IEEE*

***Abstract*—In this paper, a partially prism-gridded finite-difference time-domain (FDTD) method is proposed for the analysis of practical microwave and millimeter-wave planar circuits. The method is featured by hybridizing the flexible prism-based finite-element method to handle the region near the curved metallization boundary and the efficient rectangular-gridded FDTD method for most of the regular region. It can be used to deal with shielded or unshielded planar components such as patch antennas, filters, resonators, couplers, dividers, vias, and various transitions between planar transmission lines. Although only representative structures, e.g., grounded via, through hole via, and coplanar waveguide to coplanar stripline transition, are analyzed in this paper, the underlined formulation is applicable to layered structures with arbitrary curved boundary in transverse direction. The accuracy of this method is verified by comparing the calculated results with those by other methods. Also, by the analysis of computational complexity, the present method is shown to be as efficient as the conventional FDTD method, with negligible overhead in memory and computation time for handling the curved boundary.**

***Index Terms*—Curved boundary, FDTD method, finite-element method, layered structure.**

## I. Introduction

THE finite-difference time-domain (FDTD) method has found a lot of applications in dealing with various electromagnetic problems. Originally developed for structures that can fit well into Cartesian coordinates [1], it suffers from significant degradation in accuracy for structures with a curved boundary due to the staircasing approximation. Several attempts have been tried to alleviate the drawback by exploiting conformity to the solution region [2]–[15]. A curvilinear coordinate system was introduced in [2] to globally model the structure of interest. As compared with the original FDTD, the scheme requires additional memory to store the coordinates and spends significantly larger computation time in updating the field, even in most of the regular region. An improved scheme is to employ the locally conformed scheme [3], [4] so as to preserve the advantages of conventional FDTD as much as possible. Relying on the integral form of Maxwell's equations, both schemes suffer from worse accuracy due to a larger discretization error of first order. In addition, special attention should be paid so as not to make the algorithm unstable. Following the same approach, a generalized Yee algorithm is recently proposed to deal with planar circuits [5], but suffers from a similar discrepancy.

The subgridding method that divides the whole solution region into several orthogonal-gridded regions with different cell sizes [6], [7] has the advantages of improved accuracy without sacrificing computational efficiency. In these schemes, fields are calculated with central finite-difference formulas and interpolated on the boundaries between different regions. Basically relying on rectangular grid, the approach may require massive small cubic cells to model arbitrary boundary or else suffer from staircasing approximation. The small cells call for a proportionally short time division for the stability consideration. In addition, the interpolation along region boundary may degrade the accuracy of the results.

To have a closer fit to the curved boundary, some define the local nonorthogonal grid near the curved surfaces and transfer the fields back and forth in the overlapping region by interpolation [8], [9]. Based on the volume integral equation in nonorthogonal regions, a better approximation for surface integration of fields is also incorporated to improve the accuracy of the results. Another special approach is to carefully choose a nonuniform rectangular mesh such that the curved boundary either coincides the mesh or intersects the mesh across the diagonal [10]. In case of a metallic boundary, it is possible to derive a modified formula for updating the magnetic field at the resultant triangular cell along the boundary. Usually, this approach involves several graded meshes, in which, a shorter time step is required in order to comply with the stability criterion.

Recently, a very versatile and accurate hybrid method is proposed that employs the conventional FDTD method for most of the regular region and introduces the tetrahedral edge-based finite-element method (FEM) to model the region near the curved surfaces [11], [12]. Numerical results of simulation validate that the hybrid method has the advantages of accuracy, flexibility, and computational efficiency.

For most microwave devices, such as planar circuits, waveguides with step transitions, and packaging interconnections, the structures can be longitudinally divided into several building layers inside which the material and conductors can be of arbitrary shape in the transverse directions. In the simplest case, such as microstrip or stripline structures with thin substrate, the problem can be approximated by a two-dimensional one. Some time-domain methods capable of modeling the curved boundary have been proposed, e.g., [13] and [14]. These methods employ

Manuscript received August 25, 1998; revised December 10, 1999. This work was supported in part by the National Science Council, R.O.C., under Grant NSC 87-2213-E002-059.

The authors are with the Department of Electrical Engineering, Graduate Institute of Communication Engineering, National Taiwan University, Taipei, Taiwan 10617, R.O.C.

Publisher Item Identifier S 0018-9480(00)02065-2.

0018–9480/00$10.00 © 2000 IEEE

a conformal mesh near the curved boundary and derive special formulas for updating the field in the irregularly shaped cells. The solution schemes are explicit, but special care should be taken in mesh arrangement so as not to make algorithm unstable.

For most general multilayer cases, Righi *et al.*has proposed an approach that hybridizes a transmission-line matrix (TLM) with the mode-matching method for the enclosed region due to the housing [15]. Capable of modeling the housing region semi-analytically, the approach can be very efficient for some layered structures, but fails to deal with curved boundary accurately and efficiently. Thus, a new approach is proposed in this paper. The mesh call for triangular cells near the curved boundary in the $x$–$y$ directions while remaining a rectangular grid in the $z$-direction. It do not involve the generation of tetrahedral cells and the relatively time-consuming matrix solution of a three-dimensional (3-D) FEM required in [12]. This novel method employs two-dimensional hybrid finite-difference (FD)–FEM–time-domain (TD) method in each layer [11] and FD method to link the relationship of fields between layers along the $z$-direction.

Following this section, the novel hybrid method for objects with arbitrary curved boundary in transverse direction is mentioned in Section II. The computational aspects such as time marching, matrix solution, and computational complexity are addressed in Section III. In Section IV, the present scheme is applied to deal with problems of via interconnections and of planar circuit transition, demonstrating its flexibility and efficiency. The accuracy is also verified by comparing the calculated results with those by other methods or experiments. Finally, brief conclusions are drawn in Section V.

## II. Prism-Gridded FEM

### A. Mesh Division

Consider an illustrative example of a microstrip line with a cylindrical grounded via [see Fig. 1(a)]. It is natural to employ a uniform grid in the $z$-direction, but the staircasing approximation involved in modeling the curved via boundary in the $x$–$y$ plane may cause a significant error. A better remedy is to employ the triangular divisions in modeling the region near the via while the regular FDTD grid elsewhere, as shown in Fig. 1(b). Consequently, along the curved boundary there are four to five layers of prism cells formed by the triangular elements in the transverse plane together with the uniform grid in the $z$-direction. Note that the region directly above the microstrip can be modeled by the conventional FDTD with a regular grid. The tangential electrical field at the surface of microstrip is zero and, consequently, the conflict of cell shape below and above the microstrip line causes no problems.

Fig. 2 shows the field discretization in a prism cell. The transverse components $\vec{E}_\rho$ are located in the layers with integer $\Delta_z$ coordinates, while the longitudinal components $E_z$ in the layers with a half-integer of $\Delta_z$. As a result, the electric-field unknowns near the interface between the FEM and FDTD regions may coincide with each other exactly. No interpolation scheme need be employed when communicating between the FEM and FDTD solutions in the overlapping region.

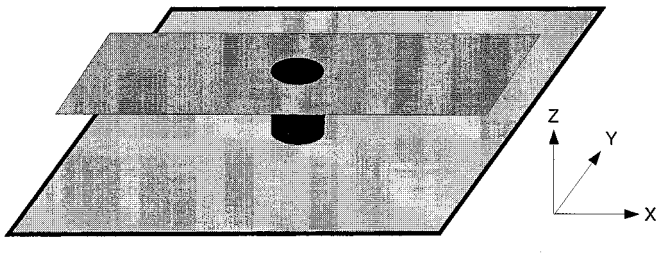


(a)

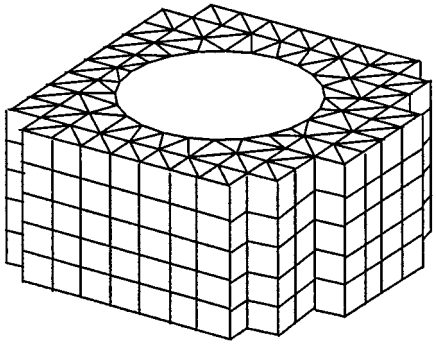

(b)

Fig. 1. (a) Geometry of microstrip with a grounded via. (b) Mesh division near and under the grounded via.

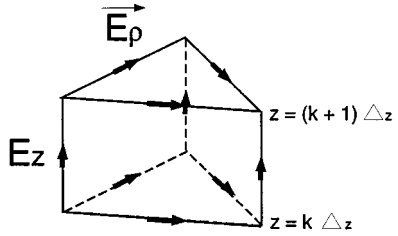


Fig. 2. Prism element and assignment of unknown fields.

### B. Weak-Form Formulation in FEM Region

Starting from the source-free Maxwell's two curl equations in a linear isotropic region, the vector-wave equation can be obtained as

$$\nabla \times \left(\frac{1}{\mu}\nabla \times \vec{E}\right) + \epsilon \frac{\partial^2 \vec{E}}{\partial t^2} = 0. \tag{1}$$

The equation can be cast into the weak form by applying the variational reaction theory [16], and considering the inner product between (1) and an arbitrary testing field $\vec{E}^a$ on one layer of the FEM region. To be more specific, choose a transversely polarized field $\vec{E}^a_\rho$ in the $z = k\Delta_z$ plane as the testing field. By performing integration by part and some algebraic simplifications, one may obtain

$$\int_A \left\{ \frac{1}{\mu}\nabla_\rho \times \vec{E}^a_\rho \cdot \nabla_\rho \times \vec{E}_\rho + \epsilon \vec{E}^a_\rho \cdot \frac{\partial^2 \vec{E}_\rho}{\partial t^2} + \vec{E}^a_\rho \cdot \left[ \frac{\partial}{\partial z}\left(\frac{1}{\mu}\nabla_\rho E_z\right) - \frac{\partial}{\partial z}\left(\frac{1}{\mu}\frac{\partial \vec{E}_\rho}{\partial z}\right)\right]\right\} dS = 0. \tag{2a}$$

Here, $\nabla_\rho \equiv \hat{x}(\partial/\partial x) + \hat{y}(\partial/\partial y)$ denotes the transverse del operator, $\vec{E}_\rho$, the transverse components of the electric field, and $E_z$, the $z$-component. Similarly, in the $z = (k + (1/2))\Delta_z$ plane, one assures that the desired field should satisfy

$$\int_A \left\{ \frac{1}{\mu} \nabla_\rho E_z^a \cdot \nabla_\rho E_z + \epsilon E_z^a \cdot \frac{\partial^2 E_z}{\partial t^2} - \frac{1}{\mu} \nabla_\rho E_z^a \cdot \frac{\partial \vec{E}_\rho}{\partial z} \right\} dS = 0 \quad (2b)$$

for the arbitrary testing field $E_z^a$.

Note that (2a) calls for the derivative of $E_z$ with respect to $z$ in the $k\Delta_z$ plane. This can be accurately approximated by using the central difference scheme, which, in the present case, requires the $E_z$ unknowns in the $(k+(1/2))\Delta_z$ and $(k-(1/2))\Delta_z$ planes. Similarly, the term $\partial \vec{E}_\rho/\partial z$ in (2b) requires the transverse unknowns $\vec{E}_\rho$ in the $k\Delta_z$ and $(k+1)\Delta_z$ planes.

### C. Basis Functions

The weak forms of (2) can be discretized into matrix forms by choosing suitable basis functions. Here, the cross-sectional area is subdivided into small triangular elements. The longitudinal component $E_z$ inside an element is expressed by node-based interpolation functions, i.e.,

$$E_z(\vec{\rho})|_{z=(k+(1/2))\Delta_z} = \sum_{i=1}^{3} \lambda_i(\vec{\rho}) e_{zi} = \{\lambda\}^T \{e_z\}_{k+(1/2)} \quad (3)$$

where $\lambda_i(\vec{\rho})$'s, $i = 1, 2, 3$ denote the three natural coordinates of the element, and $e_{zi}$'s the nodal unknowns. On the other hand, the transverse component $\vec{E}_\rho$ is expanded by

$$\vec{E}_\rho(\vec{\rho})|_{z=k\Delta_z} = \sum_{i=1}^{3} \vec{W}_i(\vec{\rho}) e_{\rho i} = \left\{\vec{W}\right\}^T \{e_\rho\}_k \quad (4)$$

where $W_i(\vec{\rho})$'s are the edge-based Whitney functions [17] and $e_{\rho i}$'s the edge unknowns. For example,

$$\vec{W}_1(\vec{\rho}) = l_{23}(\lambda_2 \nabla \lambda_3 - \lambda_3 \nabla \lambda_2)$$

$e_{\rho 1}$ is the average tangential-field component along the side from nodes 2 to 3, and $l_{23}$ is the side length.

Taking integration with respect to the basis functions and applying the Ritz procedure, one may reduce (2) to two systems of coupled differential equations for transverse and longitudinal components. This is a normal FEM solution approach and can be referred to typical textbooks, e.g., [17].

### D. Matrix Equations

The remaining terms need to be discretized in (2), which is the differentiation with respect to time. Based on the Crank–Nicolson scheme, we apply the central FD method with respect to the $t$ variable and, in addition, take timing average for the first term in (2) to achieve unconditional stability [12]. The final time-marching equations in the FEM region are

$$\begin{aligned}\left[G_{\rho\rho}^{+}\right]\{e_\rho\}_k^{n+1} = {} & 2\left[G_{\rho\rho}^{-}\right]\{e_\rho\}_k^n - \left[G_{\rho\rho}^{+}\right]\{e_\rho\}_k^{n-1} \\ & - [C_{\rho z}]\left(\{e_z\}_{k+(1/2)}^n - \{e_z\}_{k-(1/2)}^n\right) \\ & + [D_{\rho\rho}]\left(\{e_\rho\}_{k+1}^n - 2\{e_\rho\}_k^n + \{e_\rho\}_{k-1}^n\right)\end{aligned} \quad (5a)$$

and

$$\begin{aligned}\left[G_{zz}^{+}\right]\{e_z\}_{k+(1/2)}^{n+1} = {} & 2\left[G_{zz}^{-}\right]\{e_z\}_{k+(1/2)}^n - \left[G_{zz}^{+}\right]\{e_z\}_{k+(1/2)}^{n-1} \\ & + [C_{\rho z}]^T\left(\{e_\rho\}_{k+1}^n - \{e_\rho\}_k^n\right)\end{aligned} \quad (5b)$$

in which

$$\begin{aligned}\left[G_{\rho\rho}^{\pm}\right] &= \int_A \epsilon_r \{\vec{W}\}\{\vec{W}\}^T \, dS \\ &\quad \pm \frac{\kappa^2}{4} \int_A \frac{1}{\mu_r} \{\nabla_\rho \times \vec{W}\}\{\nabla_\rho \times \vec{W}\}^T \, dS \\ [C_{\rho z}] &= \kappa^2 \int_A \frac{1}{\mu_r} \{\vec{W}\}\{\nabla_\rho \lambda\}^T \, dS \\ [D_{\rho\rho}] &= \kappa^2 \int_A \frac{1}{\mu_r} \{\vec{W}\}\{\vec{W}\}^T \, dS \\ \left[G_{zz}^{\pm}\right] &= \int_A \epsilon_r \{\lambda\}\{\lambda\}^T \, dS \\ &\quad \pm \frac{\kappa^2}{4} \int_A \frac{1}{\mu_r} \{\nabla_\rho \lambda\}\{\nabla_\rho \lambda\}^T \, dS.\end{aligned}$$

Here, $\kappa = (\Delta_t/\sqrt{\mu_0 \epsilon_0}\Delta)$ is the stability factor, the superscript of $\{e_\rho\}$ and $\{e_z\}$ stands for the time step, while the subscript denotes the layer index in the $z$-direction.

### E. Discussion on Computational Efficiency

It is interesting to compare the computational load between the present method and the hybrid FDTD methods proposed in [12], [18] when applying for layered structures. For simplicity, consider the structure shown in Fig. 1(a). The region around the via is discretized into prism grids, as shown in Fig. 1(b), and solved by the FEM. Note that the cross section of each layer is identical, hence, the matrices depicted in (5) need be stored and preprocessed for one layer only during numerical simulation. Even for more general structures with several different kinds of layers, the memory requirement for the present method is much smaller than that for the other two hybrid FDTD methods.

As to the computation time, the present method that is based on the Cholesky LU decomposition method [19] as employed in [11], for each layer is superior to the hybrid method in [12], which is based on the conjugate gradient method. At each time step, the present method involves an efficient forward substitution followed by backward substitution. The operation count for each substitution equals the number of unknowns multiplied by the bandwidth of the matrices, which is estimated to be about ten [11] for most structures. On the contrary, the other two hybrid FDTD methods, which call for matrix solution for a 3-D problem are much more time consuming. At each time step,

there are usually quite a few iterations of matrix vector multiplication until convergence. It also deserves mentioning that the number of unknowns involved in the present prism gridded mesh is about half of that in the tetrahedral gridded mesh [12] since the tetrahedral mesh will introduce additional unknowns. This contributes much to the advantage of the present method.

## III. Computational Aspects

### A. Time-Marching Scheme

Separate time-domain analyses are employed for solving the Maxwell's equations in the FDTD and FEM regions. However, some type of handshaking process is required to transfer back and forth the computed data for the interface of the two regions. The time-marching scheme for the hybrid method is similar to that described in [12], except that the electric fields in the FEM region are computed by (5) layer by layer at each time step.

For example, to obtain the transverse electric field on the $k$th layer $\{e_\rho\}_k$ at time step $n+1$ by (5a), one calls for the values on neighboring layers in previous two time steps as initial conditions or, more specifically, $\{e_\rho\}_{k-1}, \{e_\rho\}_k, \{e_\rho\}_{k+1}, \{e_z\}_{k-(1/2)}, \{e_z\}_{k+(1/2)}$ at time step $n$ and $\{e_\rho\}_k$ at time step $n-1$. In addition, one require the given transverse electric fields along the boundary of the FEM region on the same layer at time step $n+1$ as the boundary conditions. These boundary conditions should be provided by the FDTD simulation in the FDTD region. Similarly, solution for the longitudinal electric field on $k+(1/2)$ layer $\{e_z\}_{k+(1/2)}$ at time step $n+1$ by (5b) requires $\{e_z\}_{k+(1/2)}, \{e_\rho\}_k, \{e_\rho\}_{k+1}$ at time step $n$ and $\{e_z\}_{k+(1/2)}$ at time step $n-1$, as well as the given nodal values on the same layer at time step $n+1$ along the boundary of the FEM region.

Once the interior fields in the FEM region are solved, the values on the contour next to the exterior boundary of the FEM region can be passed to the FDTD region for the updating of the magnetic field at the next half time step. The electric fields in the FDTD region at time step $n+2$ can then be obtained and the whole time-marching procedure continues.

### B. Matrix Solution

The unknown fields $\{e_\rho\}$ and $\{e_z\}$ in the FEM region need be solved by (5) implicitly at each time step. The matrices $[G^+_{\rho\rho}]$ and $[G^+_{zz}]$ remain the same, while right-hand-side (RHS) vectors change versus time step. The Gaussian elimination method based on Cholesky LU decomposition [19] is especially advantageous for the present case of multiple RHS vectors. In the pre-processing, the matrices $[G^+_{\rho\rho}]$ and $[G^+_{zz}]$ are decomposed into multiplication of a lower triangular and a upper triangular matrices. The matrix decomposition is time consuming, but requires to be executed once. The unknown fields at each time step can then be obtained by forward and backward substitution, which is an explicit updating scheme like FDTD. The operation count for each unknown by either the forward or backward substitution is proportional to the bandwidth of the matrices. For the storage of the matrices, the skyline scheme of variable bandwidth is employed. In addition, the unknowns are renumbered appropriately by the Collin's algorithm [20] so as to reduce the largest bandwidth.

### C. Absorbing Boundary Condition

The present hybrid method can be applied to deal with both shielded and unshielded problems. In the shielded cases, where the perfect electric conductor (PEC) planes coincide with the top and bottom surfaces of the FEM region, the Dirichlet boundary condition is employed without difficulty.

In the unshielded cases, some sort of absorbing boundary conditions should be employed to reduce the wave reflection that resulted from the artificial lattice truncation. For some examples, e.g., the grounded via structure shown in Fig. 1, the FEM region is bounded to a finite size not only in the transverse direction, but also the $z$-direction. As a result, all the exterior space is modeled by the conventionally FDTD and all the available absorbing boundary conditions can be directly resorted to. For other examples, the FEM region may be required to extend to the top and bottom layers where (5) is not applicable for lack of the fields in the next layers. Some absorbing boundary conditions, e.g., the perfectly matched layer method [21], may fail for the present case in which the cell is not rectangular in the transverse directions. Nonetheless, other absorbing boundary conditions, e.g., the first-order Mur's scheme [22], which rely on a uniform division in the direction normal to the boundary, can be employed. Additionally, on the boundary of the FDTD region elsewhere, the super-absorbing method [23] can be incorporated to further absorb the undesired reflections from the lattice truncation boundary.

### D. Computational Complexity

It is interesting to investigate the computational complexity of the additional FEM processing as compared with the conventional FDTD method. This can be treated as the overhead required by the FEM in improving the solution accuracy. To facilitate the analysis, consider the example of the grounded via structure shown in Fig. 1(a). Choosing a smaller FDTD division size $\Delta$ will increase the number of division $N_\Delta$ in each direction. The total number of variables $N$ and, thus, the required memory for FDTD in the regular region, is in the cubic order of $N_\Delta$ or written as $N = O(N_\Delta^3)$. The number of divisions required to model the curved surface is proportional to $N_\Delta$, while that in the normal direction remains nearly invariant. As a result, the number of unknowns in FEM region is $N_{\rm FEM} = O(N_\Delta^2)$. Arguably, the memory required for storing the matrices in (5) is comparatively small. One needs to store the matrix elements for one layer only. The memory requirement is roughly $B \cdot N_\Delta$, where $B$ is the average bandwidth and, in this case, remains nearly the same as $N_\Delta$ increases. Therefore, the dominant part is the storage for the additional unknowns and the FEM overhead in memory is $O(1/N_\Delta) = O(N^{-(1/3)})$.

As for the computation time, the present hybrid analysis additionally requires FEM preprocessing for the matrix setup and the matrix solution at each time-marching step. The FEM preprocessing includes the housekeeping management for mesh, element integration, matrix assembly, and the last, but usually the most time consuming, matrix decomposition into the LU form. Since it need only be done once and with the largest operation count proportional to $B^2 \cdot N_\Delta$, the required time is negligible as compared with the total simulation time. During the time

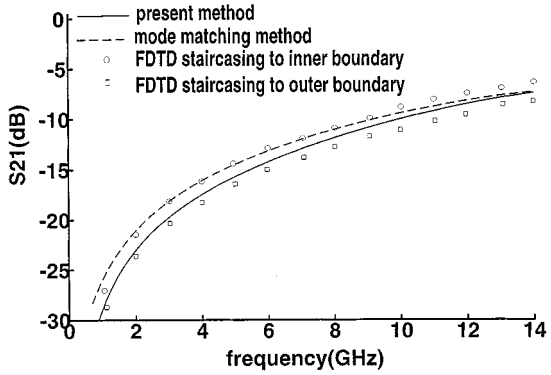


Fig. 3. Transmission coefficient along a microstrip with grounded via. Comparison between the present method and other numerical methods. The microstrip is of width 2.3 mm and height 0.8 mm, the via diameter is 0.6 mm, and the substrate is of dielectric constant 2.32. The solution region is basically divided into $110 \times 70 \times 30$ cells ($\Delta = 0.1$ mm, $\Delta_t = 1.67$ ps) with eight perfectly matched layers.

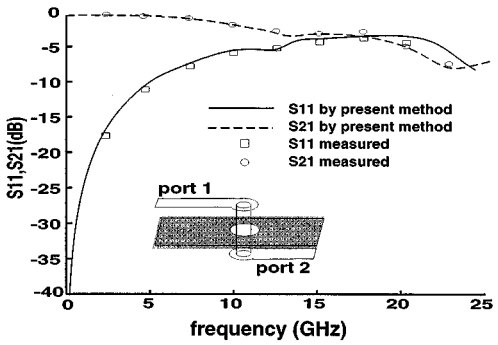


Fig. 4. Scattering parameters of a through-hole via. Comparison is between the simulated results and the measured data. The microstrip is of width 1.6 mm and height 3.3 mm, the diameters of the rod and the clearance hole are 1.5 and 3.9 mm, respectively, and the substrate is of dielectric constant 3.4. The simulation region is basically divided into $70 \times 80 \times 48$ cells with $\Delta_x = \Delta_y = 0.206$ mm, $\Delta_z = 0.4$ mm, and $\Delta_t = 0.333$ ps.

marching, the unknowns in the FEM region at each time step is solved by forward and backward substitution with operation count proportional to $2B \cdot N_{\mathrm{FEM}}$. Since $B$ is almost independent of $N_\Delta$, the FEM overhead in computation time turns out to be $O(2BN_{\mathrm{FEM}}/N_\Delta^3) = O((1/N_\Delta)) = O(N^{-(1/3)})$.

## IV. Numerical Results

### A. Grounded Via

The hybrid method is employed to characterize the microstrip with cylindrical grounded via shown in Fig. 1(a). The region around and under the rod is modeled by prism-gridded FEM. Fig. 3 compares the calculated scattering parameters with those by two staircasing FDTD analyses [18], for which one staircases the via to the inner boundary, while the other staircases the via to the outer boundary. As expected, the results by the present hybrid method lie somewhere in between. The dashed curve also shown in the figure for comparison is redrawn from the literature [24], which is based on the mode-matching method, but assuming an outer shielding box. Good agreement can be noticed.

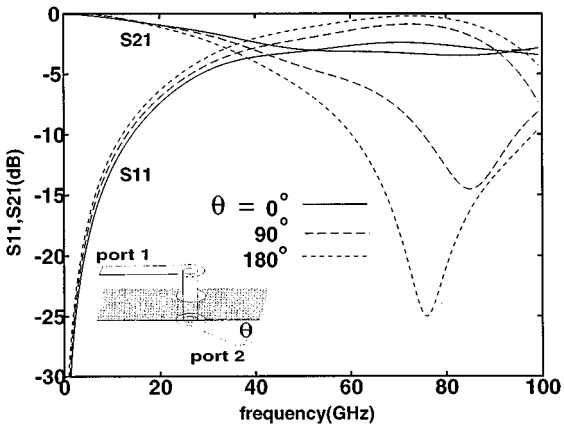


Fig. 5. Calculated scattering parameters of a through hole via with connecting angle $\theta = 0°$, $90°$, and $180°$ as a parameter. The microstrip is of width 0.254 mm and height 0.239 mm, the diameters of the via and clearance hole are 0.254 mm and 0.508 mm, respectively, and the substrate is of dielectric constant 4.3. The solution region is basically divided into $86 \times 56 \times 48$ cells with $\Delta_x = \Delta_y = 0.02117$ mm, $\Delta_z = 0.05959$ mm, and $\Delta_t = 0.0353$ ps.

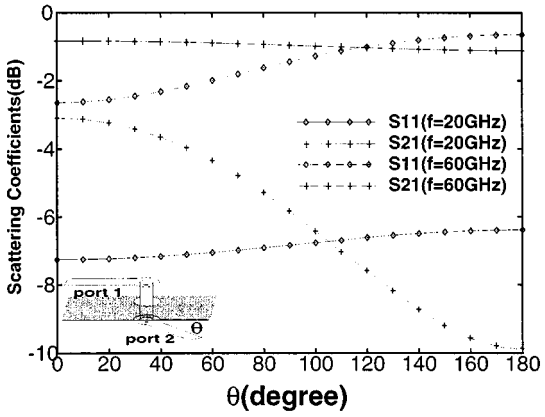


Fig. 6. Scattering parameters versus the connecting angle $\theta$ with the frequency $= 20$ GHz and $60$ GHz. All other structural parameters are the same as those in Fig. 5.

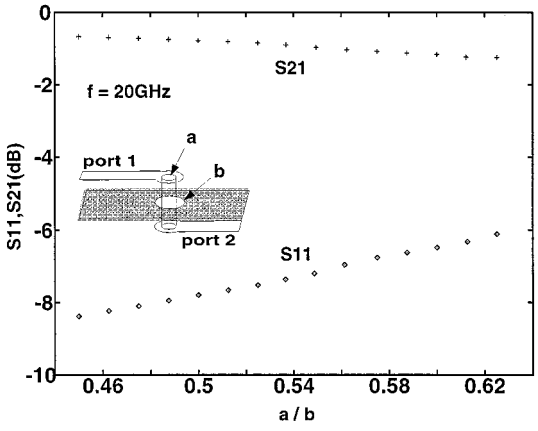


Fig. 7. Scattering parameters versus the diameter ratio of via to hole at frequency $= 20$ GHz. The via diameter is chosen as a parameter, while all others are the same as those in Fig. 5.

### B. Through Hole Via

The second example considered here is the signal transmission across the microstrip lines on different layers by a through

hole via, as shown in the inset of Fig. 4. The region near the curved boundary is discretized into prism cells and solved by the FEM, with the fields in the top and lower layers approximated by first-order Mur's boundary condition [22]. The region elsewhere is handled by the conventional FDTD, with a super-absorbing [23] first-order Mur boundary condition for the lattice truncation. Fig. 4 compares the calculated results with those by the measurement [25]. Good agreement verifies that the present method is capable of characterizing objects with curved boundary.

It is interesting to investigate the influence on scattering characteristics if the two connected lines are oriented along different directions. The structure is shown in the inset of Fig. 5. Note that the geometric parameters chosen here are typical for realistic applications in multichip modules. The characteristic impedance of the microstrip is about 50 $\Omega$. The simulation approach is similar to the previous example. Fig. 5 shows the scattering parameters versus frequency with connecting angle $\theta = 0°$, $90°$, and $180°$ as a parameter. It is found that the transmission remains good and almost independent of $\theta$ at low frequencies, say, $f < 10$ GHz. This supports the formulation and conclusions in [26], which assumes a symmetric field distribution on the clearance hole. It is also noticed that the transmission characteristics of the through-hole via degrade significantly at high frequencies, say, $f > 60$ GHz. The degradation is strongly dependent on the connecting angle $\theta$. In those cases, the diameter of the clearance hole can be as large as one-quarter of the wavelength. The field distribution around the via becomes highly asymmetric and should be carefully modeled to yield accurate results.

In case of an arbitrary connecting angle $\theta$ other than 0°, 90°, and 180°, no proper rectangular grid in the FDTD region can fit the two microstrip lines simultaneously. The problem is divided into two subregions, one is above the ground plane, while the other is below the ground plane. In general, the FDTD grids for the two subregions are tilt from each other. Notice that the two subregions overlap on the clearance around the via on the ground plane. Through the present method, we can carefully arrange different buffer meshes in these two subregions so that the identical triangular mesh on the clearance area can match to their individual FDTD grid on the outer boundary. Hence, the communication between those two subregions can be established by transferring the values of the unknowns on the clearance area to each other at each time step. Fig. 6 shows the calculated scattering parameters versus the connecting angle $\theta$ with the frequency $f = 20$ GHz and $f = 60$ GHz as a parameter.

Fig. 7 shows the calculated scattering parameters at 20 GHz with the diameter of the via as a parameter while fixing $b = 0.508$ mm. The conventional FDTD may find difficulties in modeling both the via and hole accurately with such an arbitrary aspect ratio. However, the present hybrid method can model planar structures of a curved boundary and yield a satisfactory resolution. It can be found that better transmission can be resulted by a thinner via, as depicted in [26].

### C. CPW to CPS Transition

The final example to be analyzed here is the coplanar waveguide (CPW) to coplanar stripline (CPS) transition with the layout shown in Fig. 8(a). This transition was proposed by [27], aiming at maximizing the bandwidth and minimizing the insertion loss. In this simulation, the spatial increments is 0.01524 mm and time increments are 0.0254 ps. The prism-gridded FEM is applied to deal with the region near the taper boundary, while the conventional FDTD is employed elsewhere, including the staircase approximation for the bond wires. Two PEC planes are placed 30 cells away from the planar circuit on the upper and lower boundaries, which do not exist in the measurement [28]. Roughly speaking, the whole simulation region is divided into $260 \times 80 \times 60$ cells with eight perfectly matched layers imposed on all the other walls. For the measurement, the transition structure of interest is placed in a back-to-back configuration. Fig. 8(b) compares the calculated scattering parameters with the measured data. Good agreement is obtained.

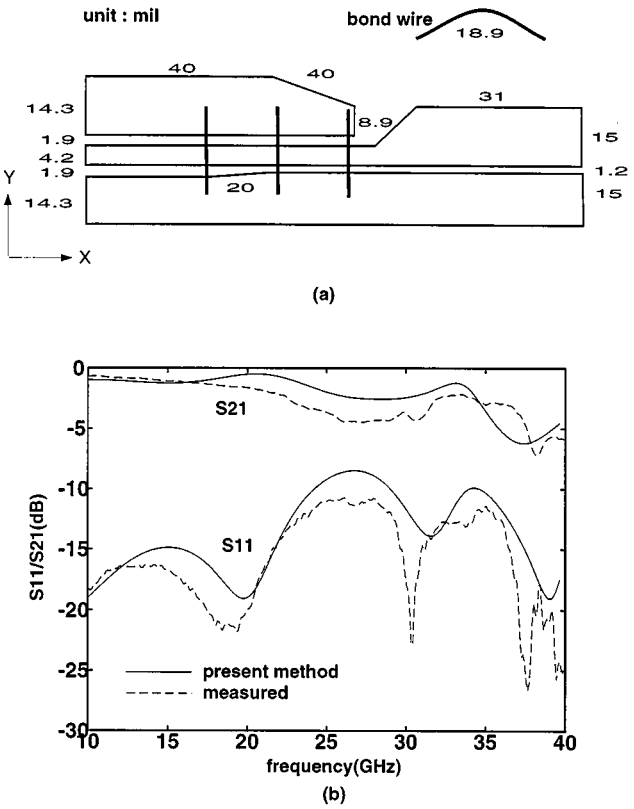


Fig. 8. (a) Layout of a CPW to CPS transition. (b) Comparison of the calculated $|S11|$ and $|S21|$ with measured data. The substrate is of height 25 mil and dielectric constant 9.8.

### D. Numerical Experiment for Computational Complexity

The experiment on computational efficiency of the present hybrid method is finally addressed. Due to the incorporation of the FEM, the method requires additional computation time and memory in mesh generation, matrix calculation, and matrix decomposition during the preprocessing, as well as in the matrix solution during the time marching. The grounded via problem described above is used as an example for a numerical experiment by tuning the division number per direction. Table I compares the required central processing unit (CPU) time and memory storage to those in the conventional FDTD algorithm. It is clearly verified that the overhead in the memory and CPU

TABLE I
COMPARISON OF THE COMPUTATION TIME AND MEMORY BETWEEN THE PRESENT METHOD AND THE CONVENTIONAL FDTD METHOD

| | mesh | | pre-processing | | time marching | | FEM overhead | |
|---|---|---|---|---|---|---|---|---|
| $\triangle$ | $N_x \times N_y \times N_z$ | method | time | memory | time/steps | memory | time | memory |
| 1.00 | $110 \times 70 \times 30$ | hybrid | 0.34 | 92 | 43.63/80 | 6580 | 14.42% | 8.51% |
| | | FDTD | - | - | 38.13/80 | 6064 | | |
| 0.80 | $138 \times 87 \times 38$ | hybrid | 0.41 | 112 | 99.63/100 | 12296 | 12.08% | 6.59% |
| | | FDTD | - | - | 88.89/100 | 11536 | | |
| 0.67 | $165 \times 105 \times 45$ | hybrid | 0.63 | 142 | 196.72/120 | 20544 | 10.01% | 5.33% |
| | | FDTD | - | - | 178.82/120 | 19504 | | |
| 0.57 | $193 \times 122 \times 53$ | hybrid | 0.78 | 164 | 353.69/140 | 32020 | 9.18% | 4.20% |
| | | FDTD | - | - | 323.94/140 | 30728 | | |
| 0.50 | $220 \times 140 \times 60$ | hybrid | 0.92 | 180 | 575.76/160 | 47072 | 7.94% | 3.77% |
| | | FDTD | - | - | 533.42/160 | 45364 | | |

time for the present hybrid method is relatively insignificant and becomes smaller for a finer mesh.

## V. CONCLUSIONS

The prism-gridded FEM has been successfully incorporated with a conventional FDTD method to deal with planar circuits with transversely curved boundary. This approach has been applied to characterize problems such as vias in packaging interconnections and transition between different transmission lines. In essence, it can also be generalized to deal with various structures such as planar circuits, waveguides with step transition, and whatever can be longitudinally divided into several building layers. Owing to the flexibility provided by the FEM, the present scheme can easily model structures with objects of arbitrary aspect ratio in shape, which is hard to access by the conventional FDTD.

The additional computational load of the present method in comparison with the conventional FDTD method has been analyzed both theoretically and numerically. In theory, the overhead of the FEM in memory and the CPU time requirement is inversely proportional to the division number per direction $N_{\triangle}$ and, thus, negligible for fine mesh. In practice, simulation results depicts that the present method remains very efficient, with computational overhead 15% smaller for most applications.

## REFERENCES


[1] K. W. Yee, "Numerical solution of initial boundary value problems in isotropic media," *IEEE Trans. Antennas Propagat.*, vol. AP-14, pp. 302–207, May 1966.

[2] R. Holland, "Finite-difference solutions of Maxwell's equation sin generalized nonorthogonal coordinates," *IEEE Trans. Nucl. Sci.*, vol. NS-30, pp. 4589–4591, Dec. 1983.

[3] T. G. Jurgens, A. Talflove, K. Umashanker, and T. G. Moore, "Finite-difference time-domain modeling of curved surfaces," *IEEE Trans. Antennas Propagat.*, vol. 40, pp. 357–366, Apr. 1992.

[4] C. H. Thng and R. C. Booton, "Edge-element time-domain method for solving Maxwell's equations," in *IEEE MTT-S Int. Microwave Symp. Dig.*, June 1994, pp. 693–696.

[5] S. Gedney and F. Lansing, "Full wave analysis of printed microstrip devices using a generalized Yee algorithm," in *IEEE AP-S Dig.*, June 1993, pp. 1179–1182.

[6] S. S. Zivanovie, K. S. Yee, and K. K. Mei, "A subgridding method for the time-domain finite-difference method to solve Maxewell's equations," *IEEE Trans. Microwave Theory Tech.*, vol. 39, pp. 471–479, Mar. 1991.

[7] D. T. Prescott and N. V. Shuley, "A method for incorporating different sized cells into the finite-difference time-domain analysis technique," *IEEE Microwave Guided Wave Lett.*, vol. 2, pp. 434–436, Nov. 1992.

[8] D. J. Riley and C. D. Turner, "Interfacing unstructured tetrahedron grids to structuted-grid FDTD," *IEEE Microwave Guided Wave Lett.*, vol. 5, pp. 284–286, Sept. 1995.

[9] K. S. Yee, J. S. Chen, and A. H. Chang, "Conformal finite-difference time-domain (FD-TD) with overlapping grid," *IEEE Trans. Antennas Propagat.*, vol. 40, pp. 1068–1075, Sept. 1992.

[10] P. Mezzanotte, L. Roselli, and R. Sorrentino, "A simple way to model curved metal boundaries in FDTD algorithm avoiding staircase approximation," *IEEE Microwave Guided Wave Lett.*, vol. 5, pp. 267–279, Aug. 1995.

[11] R. B. Wu and T. Itoh, "Hybridizing FD-TD analysis with unconditionally stable FEM for objects of curved boundary," in *IEEE MTT-S Int. Microwave Symp. Dig.*, May 1995, pp. 833–836.

[12] ——, "Hybrid finite-difference time-domain modeling of curved surfaces using tetrahedral edge elements," *IEEE Trans. Antennas Propagat.*, vol. 45, pp. 1302–1309, Aug. 1997.

[13] W. K. Gwarek, "Analysis of an arbitrarily-shaped planar circuit-a time-domain approach," *IEEE Trans. Microwave Theory Tech.*, vol. 33, pp. 1067–1072, Oct. 1985.

[14] A. C. Cangellaris, C. C. Lin, and K. K. Mei, "Point-matched time domain finite-element methods for electromagnetic radiation and scattering," *IEEE Trans. Antennas Propagat.*, vol. AP-35, pp. 1160–1173, Oct. 1987.

[15] M. Righi, J. L. Herring, and W. J. R. Hoefer, "Efficient hybrid TLM/mode-matching analysis of packaged components," *IEEE Trans. Microwave Theory Tech.*, vol. 45, pp. 1715–1724, Oct. 1997.

[16] R. B. Wu, "A wide-band waveguide transition design with modified dielectric transformer using edge-based tetrahedral finite element analysis," *IEEE Trans. Microwave Theory Tech.*, vol. 44, pp. 1024–1031, July 1996.

[17] J. Jin, *The Finite Element Method in Electromagnetics*. New York: Wiley, 1993, sec. 2.1, 4.3, 8.1.

[18] D. Koh, H. B. Lee, and T. Itoh, "A hybrid full-wave analysis of via hole grounds using finite difference and finite element time domain methods," in *IEEE MTT-S Int. Microwave Symp. Dig.*, June 1997, pp. 89–92.

[19] K. J. Bathe and E. L. Wilson, *Numerical Methods in Finite Element Analysis*. Englewood Cliffs, NJ: Prentice-Hall, 1976, sec. 7.2.4.

[20] R. J. Collins, "Bandwidth reduction by automatic renumbering," *Inform. J. Numer. Method Eng.*, vol. 6, pp. 345–356, 1973.

[21] J. P. Berenger, "A perfectly matched layer for the absorption of electromagnetic waves," *J. Comput. Phys.*, vol. 114, pp. 185–200, Oct. 1994.

[22] G. Mur, "Absorbing boundary conditions for the finite-difference approximation of the time-domain elecytromagnetic-field equations," *IEEE Trans. Electromag. Compat.*, vol. EC-23, pp. 377–382, Nov. 1981.

[23] K. K. Mei and J. Fang, "Superabsorption—A method to improve absorbing boundary conditions," *IEEE Trans. Antennas Propagat.*, vol. 40, pp. 1001–1010, Sept. 1992.

[24] R. Sorrentino, F. Alessandri, M. Mongiardo, G. Avitabile, and L. Roselli, "Full-wave modeling of via hole grounds in microstrip by three-dimensional mode matching technique," *IEEE Trans. Microwave Theory Tech.*, vol. 40, pp. 2228–2234, Dec. 1992.

[25] S. Maeda, T. Kashiwa, and I. Fukai, "Full wave analysis of propagation characteristics of a through hole using the finite-difference time-domain method," *IEEE Trans. Microwave Theory Tech.*, vol. 39, pp. 2154–2159, Dec. 1991.

[26] S. G. Hsu and R. B. Wu, "Full wave characterization of a through hole via in miltilayered packaging," *IEEE Trans. Microwave Theory Tech.*, vol. 43, pp. 1073–1081, May 1995.

[27] H. K. Chiou, C. Y. Chang, and H. H. Lin, "Balun design for uniplanar broad band double balanced mixer," *Electron. Lett.*, vol. 31, pp. 211–212, Nov. 1995.
[28] S. G. Mao, C. T. Hwang, R. B. Wu, and C. H. Chen, "Analysis of coplanar waveguide-to-coplanar stripline transitions," IEEE Trans. Microwave Theory Tech., submitted for publication.

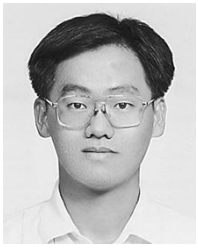

**Chieh-Tsao Hwang** was born in Tainan, Taiwan, R.O.C., in 1968. He received the B.S. in physics, and the M.S. and Ph.D. degrees in electrical engineering from the National Taiwan University, Taipei, Taiwan, R.O.C., in 1991, 1993, and 1999, respectively.

His area of interest include computational electromagnetics, transmission-line discontinuities, and electromagnetic theory.

**Shau-Gang Mao** (S'97–M'98) was born in Kaohsiung, Taiwan, R.O.C., on October 11, 1970. He received the B.S. degree in atmosphere science, and the M.S.E.E. and the Ph.D. degrees in electrical engineering from the National Taiwan University, Taipei, Taiwan, R.O.C., in 1992, 1994, and 1998, respectively.

His research interests include the design and analysis of uniplanar microwave active and passive components.

**Ruey-Beei Wu** (M'91–SM'97) was born in Tainan, Taiwan, R.O.C., in 1957. He received the B.S.E.E. and Ph.D. degrees from the National Taiwan University, Taipei, Taiwan, R.O.C., in 1979 and 1985, respectively.

In 1982, he joined the faculty of the Department of Electrical Engineering, Graduate Institute of Communication Engineering, National Taiwan University, where he is currently a Professor. From March 1986 to February 1987, he was a Visiting Scholar at IBM, East Fishkill, NY. From August 1994 to July 1995, he was with the Electrical Engineering Department, University of California at Los Angeles. Since 1998, he has been the Director of the National Center for High-Performance Computing, National Science Council, R.O.C. His areas of interest include computational electromagnetics, dielectric waveguides, edge-slot antennas, wave scattering of composite materials, transmission-line discontinuities, and interconnection modeling for computer packaging.

**Chun-Hsiung Chen** (SM'88–F'96) was born in Taipei, Taiwan, R.O.C., on March 7, 1937. He received the B.S.E.E. degree from the National Taiwan University, Taipei, R.O.C., in 1960, the M.S.E.E. degree from the National Chiao Tung University, Hsinchu, Taiwan, R.O.C., in 1962, and the Ph.D. degree in electrical engineering from the National Taiwan University, Taipei, R.O.C., in 1972.

In 1963, he joined the Faculty of the Department of Electrical Engineering, National Taiwan University, where he currently a Professor. From August 1982 to July 1985, he was Chairman of the Department of Electrical Engineering, National Taiwan University, and from August 1992 to July 1996, he was the Director of the University Computer Center. In 1974, he was a Visiting Researcher for one year in the Department of Electrical Engineering and Computer Sciences, University of California at Berkeley. From August 1986 to July 1987, he was a Visiting Professor in the Department of Electrical Engineering, University of Houston, Houston, TX. In 1989, 1990, and 1994, he visited the Microwave Department, Technical University of Munich, Munich, Germany, Laboratoire d'Optique Electromagnetique, Faculte des Sciences et Techniques de Saint-Jerome, Universite d'Aix-Marseille III, France, and the Department of Electrical Engineering, Michigan State University, East Lansing, respectively. His areas of interest include antenna and waveguide analysis, propagation and scattering of waves, and numerical techniques in electromagnetics.